Crystalline Structure and Lithium-Ion Channel Formation in Self-Assembled Di-lithium Phthalocyanine: Theory and Experiments

Yingchun Zhang,[†] Paula R. Alonso,[†] Alberto Martinez-Limia,[†] Lawrence G. Scanlon,[‡] and Perla B. Balbuena*[,†]

Department of Chemical Engineering, University of South Carolina, Columbia, South Carolina 29208, and Air Force Research Laboratory, Energy Storage & Thermal Sciences Branch, Wright-Patterson Air Force Base, Ohio 45433

Received: November 2, 2003; In Final Form: January 28, 2004

The crystalline structure of di-lithium phthalocyanine (Li_2Pc) is analyzed via a sequence of theoretical methods starting with ab-initio optimizations of a single molecule and dimers, followed by a series of classical molecular dynamics simulations that emulate four alternative crystalline structures. Calculated X-ray spectra are compared with those from experiments, and the results suggest that the features correspond to a dominant β-phase, although similarities in the calculated spectrum of alternative phases may imply the possible existence of polymorphism in this material. Since Li_2Pc has been proposed as a solid electrolyte for lithium-ion batteries, the existence of ion-conducting channels is examined through the analyses of the simulated structures. Dynamical properties such as the lithium-ionic diffusion coefficient are determined through the velocity autocorrelation function and compared to experimental values.

1. Introduction

Di-lithium phthalocyanine (Li_2Pc), as shown in Figure 1, has been proposed as a solid electrolyte for lithium-ion batteries, with the expected advantage of providing single-ion transport characteristics for lithium ions.[1] Molecular self-assembly may lead to the formation of lithium ion conducting channels, where the anion matrix of di-lithium phthalocyanine, an unsaturated macrocyclic compound, forms the channel. When such a self-assembled structure is used as the solid electrolyte of lithium-ion batteries, lithium ion transport may depend on the electric field gradient established between the electrodes, instead of being a function of polymer segmental motion as that observed for oxygen-based solid polymer electrolytes, and therefore, it is expected that the temperature dependence for lithium ion conduction will be minimized. Also, voltage drop across the electrolyte will be minimized even at high current loads because of the single-ion transport characteristics. The performance of Li_2Pc as electrolyte in an all-solid state electrochemical cell has been recently reported.[2]

In view of the potential advantages of the use of Li_2Pc as a solid electrolyte, understanding the lithium-ionic transport mechanisms in solid Li_2Pc becomes essential. However, little is known about its crystalline structure. Other metal phthalocyanines are known to be polymorphic.[3−13] Particularly, a great deal of research has been done on the polymorphism of lithium phthalocyanine because of its potential use as an oximetry probe and its interesting electrical and magnetic behavior.[7,8] Depending on the preparation conditions, LiPc can crystallize in three different structures, namely, α-, β-, and χ-forms. The α- and β-forms of LiPc show monoclinic unit cells with parameters a = 2.57 nm, b = 0.38 nm, c = 2.36 nm, and β = 91.0° and space group $C2/c$,[14] and a = 1.94 nm, b = 0.49 nm, c = 1.40 nm, and β = 120.36° and space group $P2_{1/c}$,[15] respectively. The χ-form shows a tetragonal unit cell with parameters $a = b$ = 1.385 nm and c = 0.65 nm and the space group $P4/mcc$.[9] These three polymorphs showed different properties correlated to the nature of molecular packing.[10]

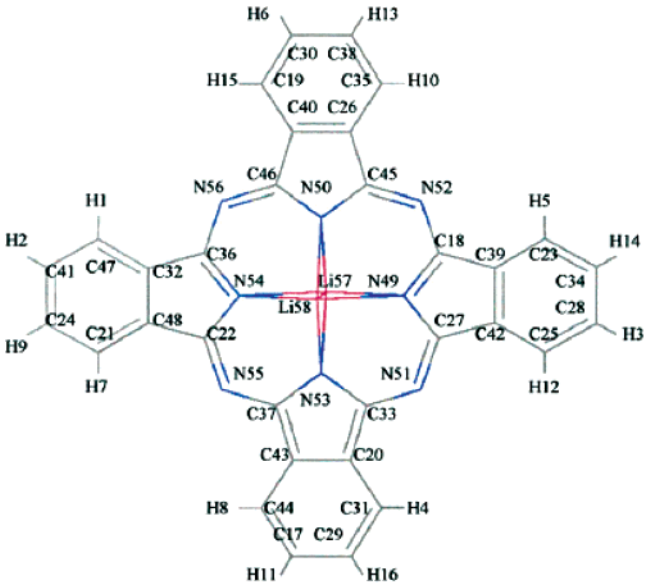

Figure 1. Li_2Pc molecule.

X-ray spectra of Li_2Pc were obtained at Argonne National Laboratory[16] and at the Air Force Laboratory where Li_2Pc solid-state density was also determined.[17] We have used this information to formulate models that, in conjunction with ab-initio data for the single molecule and dimers are input for classical molecular dynamics (MD) simulations used to investigate self-assembled structures and determine their corresponding X-ray spectra. We focus on the characterization of structural and

* Author to whom correspondence should be addressed. E-mail: balbuena@engr.sc.edu.
[†] University of South Carolina.
[‡] Wright-Patterson Air Force Base.

10.1021/jp037322k CCC: $27.50
Published on Web 03/20/2004

TABLE 1: Cell Parameters of α-, *β*-, *ϵ*-, and *χ*-Forms of Li_2Pc Used in MD Simulations

crystalline structure	*a* (Å)	*b* (Å)	*c* (Å)	α (°)	*β* (°)	*γ* (°)
α	26.2	4.0	23.9	90.0	94.5	90.0
β	19.4	5.1	14.6	90.0	120.4	90.0
ϵ	5.1	14.0	18.3	118.2	90.0	90.0
χ	13.8	13.8	6.5	90.0	90.0	90.0

dynamical properties of a self-assembly of Li_2Pc and its potential to provide lithium-ion conducting channels for lithium-ion batteries. Calculated X-ray spectra and lithium-ion diffusion coefficients are compared to experimental results. The possibility of the existence of ion-channels in the solid-state structure is investigated through analyses of configurations derived from the MD simulations.

2. Computational Details

2.1. Ab-Initio Calculations. Hartree−Fock (HF) and density functional theory (DFT) geometry optimizations were performed on a single Li_2Pc molecule (Figure 1) and on dimers in shifted and staggered structures, to determine their main geometrical and electronic characteristics. Full optimizations were performed at the HF/6-311G, B3PW91/6-311G, and B3LYP/6-31G(d) levels, using the program Gaussian 98.[18] The geometry and charge distribution obtained for a single molecule at B3PW91/6-311G level is used as input for MD simulations.

2.2 Molecular Dynamics Simulations. *2.2.1. Initial Configurations*. Four primitive unit cells (designated as α-, *β*-, *ϵ*-, and *χ*-forms) were built on the basis of several sources of data for this and related systems: (1) the analysis of experimental X-ray spectra of crystalline Li_2Pc,[16] (for the *ϵ*-form); (2) the experimental density of solid Li_2Pc at room temperature[17] (for the α-, *β*-, and *χ*-forms); and (3) the reported polymorphism of various metal phthalocyanines[7,8,10] (for the α-, *β*-, and *χ*-forms). The cell parameters of the four configurations are shown in Table 1. Among these polymorphs, the α-, *β*-, and *ϵ*-form structures have monoclinic unit cells, and the *χ*-form has a tetragonal unit cell. The primitive unit cells for the α-, *β*-, and *χ*-forms have the same dimensions as the reported structures for the polymorphs of LiPc except that the shortest cell dimension was elongated to fit the experimental density of Li_2-Pc (1.40 g/cm^3). The cell parameters of the *ϵ*-form were chosen to match the crystal *d* spacing that best reproduces the experimental X-ray data, as calculated with the powder indexing program CRYSFIRE 2002.[19]

The starting configurations for the MD simulations of the α-, *β*-, *ϵ*-, and *χ*- crystalline forms are shown in Figure 2. All initial configurations were set in staggered arrangements, and in the *χ*-form molecules in subsequent layers are rotated with respect to each other by an angle of 30° (Figure 3) according to structures reported for pthalocyanines[6] and also based in our ab-initio calculations of Li_2Pc dimers.

The initial geometry of the individual Li_2Pc molecules used in the MD simulations was taken from the DFT optimized structure of a single molecule (B3PW91/6-311G). The unit cells shown in Table 1 were duplicated along the shortest cell length to define the initial MD simulation cell for each of the Li_2Pc forms. As a result, MD simulation cells of the α- and *χ*-forms contained 24 Li_2Pc molecules, whereas those of the *β*- and *ϵ*-forms contained 32 Li_2Pc molecules (Figure 2). To minimize strain of the initial configurations, a total energy minimization was performed previous to the MD simulations using the UFF force field,[20] and a combination of minimization methods (steepest descent, adopted basis Newton Raphson, Quasi Newton, and Truncated Newton) were applied as provided in the Cerius^2 3.0 package.[21] The minimized ensembles were used as input to the DL-POLY program,[22] to perform MD simulations using the force fields described in the next section.

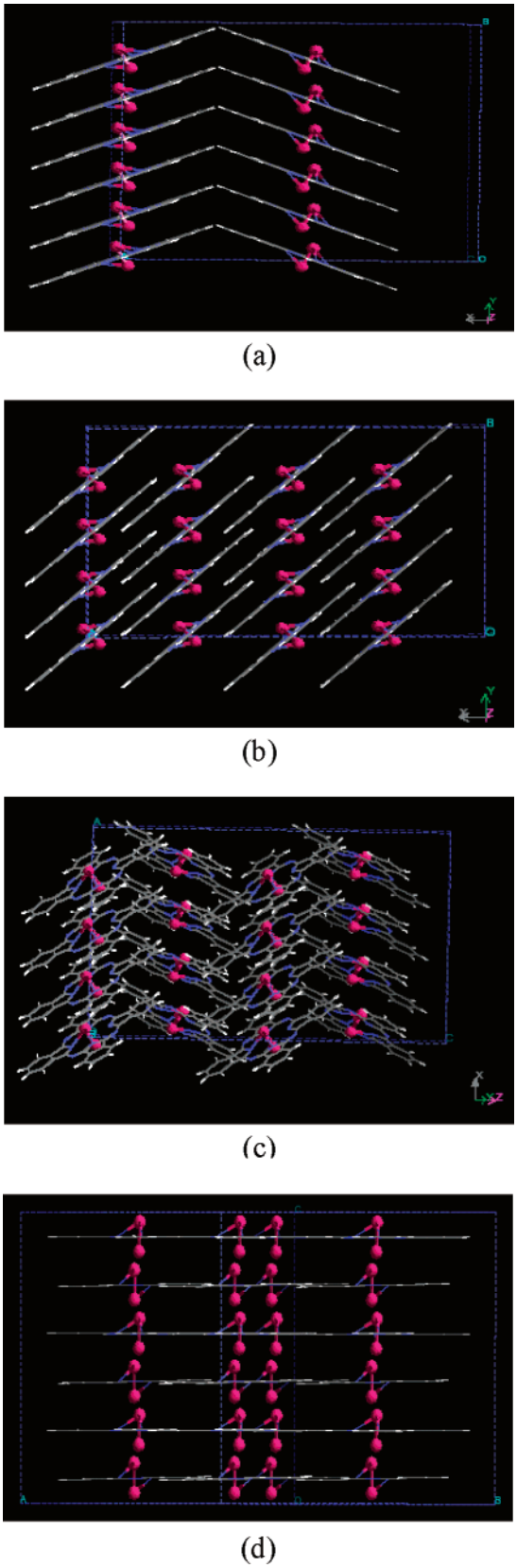

Figure 2. Initial configuration of the unit cells for molecular dynamics simulations (a) α-form, (b) *β*-form, (c) *ϵ*-form, (d) *χ*-form.

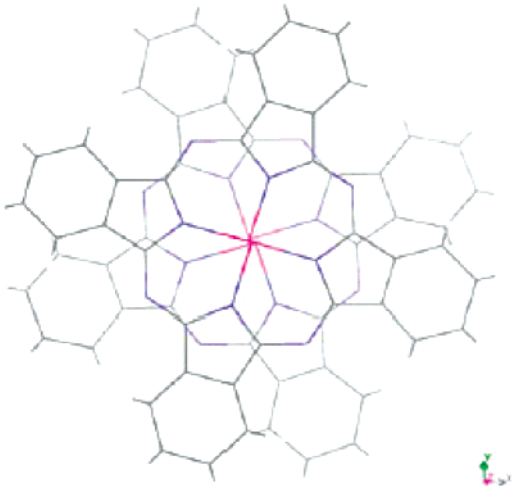

Figure 3. Rotation of two dilithium phthalocyanine molecules used for the initial configuration of the χ-form.

2.2.2. Force Fields. The selected force field contains intramolecular and intermolecular terms. The *intramolecular* potential includes the following two terms: (1) Bond potential:

$$U(r_{ij}) = \frac{1}{2}k_{ij}(r_{ij} - r_{ij,0})^2 \quad (1)$$

(2) Valence angle potential:

$$U(\theta_{jik}) = A_{jik}[1 + \cos(m_{jik}\theta_{jik} - \delta_{jik})], \quad (2)$$

where k_{ij} and A_{jik} are force constants relating atoms i, j, and k, r_{ij} is the distance between atoms i and j ($r_{ij} = |\bar{r}_i - \bar{r}_j|$), $r_{ij,0}$ is the corresponding equilibrium distance, and θ_{jik} is the angle between bond vectors $\bar{r}_{ij}$ and $\bar{r}_{ik}$.

The force constants for the potential terms were evaluated according to the following equations[20] where the parameters $r_{ij,0}$, and θ_0 (Table 2) were obtained averaging over all atoms (bonds, or angles) of the same type from the optimized geometry of Li_2Pc calculated with B3PW91/6-311G, whereas the parameter z_i^* was taken as the Mulliken atomic charge obtained also from the DFT calculation of a single molecule (average atomic charges are reported in Table 4):

$$k_{ij} = 664.12\frac{z_i^* z_j^*}{r_{ij,0}^3}\frac{\text{kcal}}{\text{mol}} \quad (3)$$

$$A_{ijk} = \frac{664.12}{r_{ij,0}r_{jk,0}}\frac{z_i^* z_k^*}{{r_{IK}}^5}r_{ij,0}r_{jk,0}[3r_{ij,0}r_{jk,0}(1 - \cos^2\theta_0) - {r_{IK}}^2\cos\theta_0]\frac{\text{kcal}}{\text{mol}} \quad (4)$$

$$r_{IK} = (r_{ij,0}^2 + r_{jk,0}^2 - 2r_{ij,0}r_{jk,0}\cos\theta_0)^{1/2} \quad (5)$$

where $m = \pi/(\pi - \theta_0)$, and $\delta = -\pi + (\pi\theta_0)/(\pi - \theta_0)$.

To allow the migration of lithium ions from the molecule, neither the bond potential between Li and N, nor the valence angle potentials among Li−N−Li and N−Li−N were included. Instead, the Li−N interaction was represented by a combination of 12-6 Lennard-Jones (LJ) and Coulombic site−site potential functions with parameters reported in Tables 3 and 4. The DFT optimized (B3PW91/6-311G) Li−N bond length is 2.18 Å, which can be compared with the value 2.17 Å obtained with this model, while the UFF[20] 12-6 LJ potential yields 2.15 Å. Although accurate descriptions of the van der Waals interactions are certainly critical for these types of compounds, the Li−N is the most critical bond distance since an explicit harmonic bond potential between Li and N is not present in our model.

The *intermolecular* potentials include two terms:

(1) A short-ranged LJ (12-6) potential:

$$U(r_{ij}) = 4\epsilon\left[\left(\frac{\sigma}{r_{ij}}\right)^{12} - \left(\frac{\sigma}{r_{ij}}\right)^{6}\right] \quad (6)$$

where ϵ is the LJ well depth in kJ/mol, and σ is the LJ length parameter in Å. The well-depth and van der Waals length parameters for interactions between H, N, and C atoms of the same type were selected as in the Dreiding force field.[23] For Li−Li interactions, we used the LJ parameters reported by Heizinger[24] (Table 3). The LJ parameters between atoms of different species were calculated with the Lorentz−Berthelot rule.[25]

(2) The Ewald sum[25] was used to incorporate long-range corrections to the usual electrostatic (Coulombic) potential. For molecular systems, the Ewald sum replaces a potentially infinite sum in real space with two finite sums: one in real space and one in reciprocal space, and the self-energy correction.[22,25] The Mulliken[26−28] atomic charges used for the Coulombic terms were obtained from DFT optimized geometries (B3PW91/6-311G) for one Li_2Pc molecule; they are shown in Table 4.[2]

2.2.3. MD Procedure. The DL_POLY program,[22] version 2.13, was used in all simulations. MD simulations were run in the microcanonical ensemble (NVE) for 1200 ps with a time step of 0.001 ps at 300 K. Equilibration runs of 500 ps were performed before collecting averages in production runs of 700 ps. During the equilibration phase, the interval for scaling velocities according to the selected temperature was set to 0.002 ps; in the production phase, the scaling is disconnected but the temperature remains about constant. The cutoff radius, beyond which intermolecular interactions of the real space part of the long-range electrostatic and the van der Waals potentials were set to zero, was chosen as 10.0 Å, which corresponds to half the minimum cell length.

3. Results and Discussion

3.1 Ab-Initio Calculations. Li_2Pc and $(Li_2Pc)_2$ were optimized using HF and DFT. Results for the single molecule obtained with B3PW91/6-311G are shown in Figure 4 and Table 5. The most relevant parameters are the distance between two lithium atoms in one Li_2Pc molecule, 1.99 Å, and the average distance between Li and each of the N atoms N49, N50, N53, and N54, is 2.18 Å. DFT optimizations of the single molecule were performed using B3PW91/6-311G and B3LYP/6-31G(d), yielding good agreement in the structural parameters.

The optimization of $(Li_2Pc)_2$ using HF/6-311G yielded a staggered configuration; the shortest distance between lithium atoms in different molecules was found to be 2.99 Å. A stacking distance of 3.7 Å was estimated from the average separation between atoms that almost overlap one another in a top view. The two molecules are rotated by an angle of approximately 30°. Both shifted and staggered dimer configurations were obtained at HF/6-31G(d); the shifted yield a PC ring separation of approximately 3.8 Å, and Li atoms from different molecules are separated by 3.19 Å, whereas the staggered dimer structure (shortest distance between Li atoms of 2.76 Å, and average stacking distance of 3.7 Å) is much less stable than the shifted form (Table 6).

TABLE 2: Selected Force Field Equilibrium Distances $r_{ij,0}$ (Å) and Angles θ_0 (degrees) Averaged over All Bonds and Angles of the Same Type, from the Values Obtained from Li_2Pc Optimization (B3PW91/6-311G). The Atom Numbers Correspond to Figure 1

i j	atom numbers for pair *i*−*j*	$r_{ij,0}$
H C	9−21, 2−41, 6−30, 13−38, 14−34, 3−28, 11−17, 16−29	1.086
H C	7−21, 1−47, 15−19, 10−35, 8−44, 4−31, 12−25, 5−23	1.085
C C	17−29, 24−41, 28−34, 30−38	1.405
C C	43−20, 32−48, 40−26, 39−42	1.401
C C	17−44, 29−31, 24−21, 41−47, 30−19, 38−35, 23−34, 25−28	1.389
C C	43−44, 20−31, 21−48, 32−47, 19−40, 26−35, 23−39, 25−42	1.392
C C	37−43, 20−33, 27−42, 18−39, 26−45, 40−46, 32−36, 22−48	1.455
C N	22−54, 36−54, 46−50, 45−50, 18−49, 27−49, 33−53, 37−53	1.370
C N	36−56, 46−56, 45−52, 18−52, 27−51, 33−51, 37−55, 22−55	1.324

i j k	atom numbers for group *i*−*j*-*k*	θ_0
C C H	48−21−7, 32−47−1, 40−19−15, 26−35−10 39−23−5, 42−25−12, 20−31−4, 43−44−8	120.68
C C H	24−21−7, 41−47−1, 30−19−15, 38−35−10 34−23−5, 28−25−12, 29−31−4, 17−44−8	121.69
C C H	21−24−9, 47−41−2, 19−30−6, 35−38−13 23−34−14, 25−28−3, 31−29−16, 44−17−11	119.67
C C H	41−24−9, 24−41−2, 38−30−6, 30−38−13 28−34−14, 34−28−3, 17−29−16, 29−17−11	119.14
C C C	22−48−21, 36−32−47, 46−40−19, 45−26,35 18−39−23, 27−42−25, 33−20−31, 37−43−44	132.71
C C C	22−48−32, 36−32−48, 46−40−26, 45−26−40 18−39−42, 27−42−39, 33−20−43, 37−43−20	106.11
C C C	21−48−32, 47−32−48, 19−40−26, 35−26−40 23−39−42, 25−42−39, 31−20−43, 44−43−20	121.18
C C C	48−21−24, 32−47−41, 40−19−30, 26−35−38 39−23−34, 42−25−28, 20−31−29, 43−44−17	117.63
C C C	21−24−41, 47−41−24, 19−30−38, 35−38−30 23−34−28, 25−28−34, 31−29−17, 44−17−29	121.19
C C N	48−22−55, 43−37−55, 32−36−56, 40−46−56 26−45−52, 39−18−52, 42−27−51, 20−33−55	122.38
C C N	48−22−54, 32−36−54, 40−46−50, 26−45−50 39−18−49, 42−27−49, 20−33−53, 43−37−53	110.22
N C N	55−22−54, 56−36−54, 56−46−50, 52−45−50 52−18−49, 51−27−49, 51−33−53, 55−37−53	127.40
C N C	37−55−22, 46−56−36, 33−51−27, 45−52−18	122.55
C N C	22−54−36, 46−50−45, 18−49−27, 33−53−37	107.34

TABLE 3: Values of LJ 12-6 Parameters

atom	ϵ (kJ/mol)	σ (Å)
H	6.35×10^{-2}	2.846
C	3.98×10^{-1}	3.473
N	7.74×10^{-1}	3.263
Li	1.50×10^{-1}	2.370

TABLE 4: Mean Values (averaged over all atoms of the same type) of the Mulliken Atomic Charges from B3PW91/6-311G Optimization of Li_2Pc[a]

atom type	atom number	charge
H	1, 4, 5, 7, 8, 10, 12, 15	0.21
	2, 3, 6, 9, 11, 13, 14, 16	0.20
C	17, 24, 28, 29, 30, 34, 38, 41	−0.20
	19, 21, 23, 25, 31, 35, 44, 47	−0.17
	20, 26, 32, 39, 40, 42, 43, 48	−0.08
	18, 22, 27, 33, 36, 37, 45, 46	0.39
N	49, 50, 53, 54	−0.63
	51, 52, 55, 56	−0.40
Li	57, 58	0.66

[a] The atom numbers correspond to Figure 1.

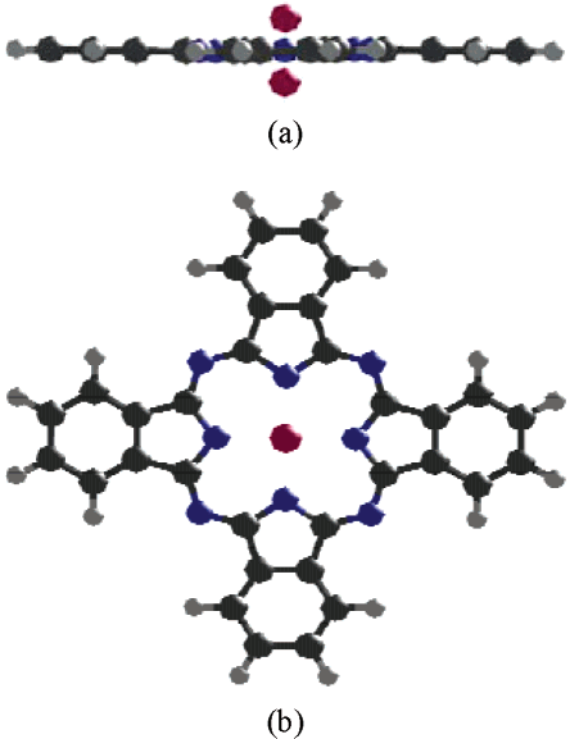

Figure 4. Structure of Li_2Pc molecule optimized with B3PW91/6-311G (a) side view, (b) top view.

Electron correlation was introduced via DFT calculations. To understand how these predictions of atomic charges and geometrical parameters (bond lengths and angles) would affect the outcome of the crystal structure, it is useful to analyze the nature of the forces involved. The intramolecular parameters of the individual Pc rings are determined by covalent forces, and strong electrostatic forces govern the intra- and intermolecular Li−N interactions. Thus, it is expected that the self-assembled structure of the crystal is primarily determined by electrostatic forces, and by weak van der Waals forces in a

TABLE 5: Optimized B3PW91/6-311G Values for Selected Bond Distances and Angles for Li_2Pc[a]

atom #	atoms	r_{ij} (Å)	atom #	atoms	θ_{ijk}	atom #	atoms	θ_{ijk}
7 21	CH	1.08	48 21 7	C C H	121.68	32 36 56	C C N	122.44
9 24	CH	1.09	7 21 24	C C H	121.69	36 56 46	C N C	122.59
2 41	CH	1.09	21 24 9	C C H	119.67	18 49 57	C N Li	122.23
1 47	CH	1.08	9 24 41	C C H	119.15	18 49 58	C N Li	121.28
22 54	C N	1.37	24 41 2	C C H	119.13	57 49 27	Li N C	121.19
36 54	C N	1.37	2 41 47	C C H	119.67	58 49 27	Li N C	122.32
36 56	C N	1.32	41 47 1	C C H	121.69	33 53 57	C N Li	122.35
22 55	C N	1.32	1 47 32	C C H	120.68	57 53 37	C N Li	122.24
54 57	N Li	2.15	22 48 21	C C C	132.70	33 53 58	C N Li	121.06
50 57	N Li	2.18	48 21 24	C C C	117.65	58 53 37	C N Li	121.33
49 57	N Li	2.20	21 24 41	C C C	121.19	54 57 53	N Li N	78.40
53 57	N Li	2.18	24 41 47	C C C	121.20	53 57 49	N Li N	78.30
54 58	N Li	2.20	41 47 32	C C C	117.63	49 57 50	N Li N	77.21
50 58	N Li	2.18	47 32 36	C C C	132.73	54 57 50	N Li N	77.78
49 58	N Li	2.15	22 48 32	C C C	106.07	54 58 53	N Li N	77.22
53 58	N Li	2.17	48 32 36	C C C	106.07	53 58 49	N Li N	77.42
57 58	Li Li	2.00	21 48 32	C C C	121.13	49 58 50	N Li N	78.45
22 48	C C	1.45	48 32 47	C C C	121.15	54 58 50	N Li N	78.33
48 21	C C	1.39	55 22 48	N C C	122.30	46 50 57	C N Li	121.15
21 24	C C	1.39	55 22 54	N C N	127.36	46 50 58	C N Li	122.29
24 41	C C	1.40	48 22 54	N C C	110.20	57 50 45	Li N C	121.40
41 47	C C	1.39	37 55 22	C N C	122.51	58 50 45	Li N C	122.15
47 32	C C	1.39	22 54 36	C N C	107.35	57 58 50	Li Li N	63.94
48 32	C C	1.40	22 54 57	C N Li	121.25	57 58 49	Li Li N	62.88
32 36	C C	1.45	36 54 57	C N Li	122.25	57 58 53	Li Li N	61.41
			22 54 58	C N Li	122.28	57 58 54	Li Li N	62.54
			36 54 58	C N Li	121.24	58 57 50	Li Li N	61.40
			54 36 32	N C C	110.20	58 57 49	Li Li N	62.46
			54 36 56	N C N	127.35	58 57 53	Li Li N	63.95
						58 57 54	Li Li N	62.82

[a] Atom numbers correspond to Figure 1.

TABLE 6: Optimized Energies (Hartrees) and Binding Energies (kcal/mol) for Li_2Pc and $(Li_2Pc)_2$

method	basis set	electronic energy Li_2Pc	electronic energy $(Li_2Pc)_2$	binding energy
HF	4-31G	−1669.35334	−3338.748964[a]	26.54
HF	6-31G	−1671.12350		
HF	6-311G	−1671.42953	−3342.88672[a]	17.36
HF	6-31G(d)	−1671.81142	−3343.64246[a]	12.31
HF	6-31G(d)	−1671.81142	−3343.66290[b]	25.14
B3PW91	4-31G	−1679.46165		
B3PW91	6-311G	−1682.02541		
B3LYP	3-21G	−1673.06456	−3346.20214[a]	45.80
B3LYP	6-31G(d)	−1682.35746	−3364.74344[a]	17.90
B3LYP	3-21G	−1673.06456	−3346.19101[b]	38.80
B3LYP	6-31G(d)	−1682.35746	−3364.74572[b]	19.30

[a] Staggered configuration. [b] Shifted configuration.

second place. DFT calculations give good estimates of charges and geometrical parameters of individual Li_2Pc molecules, which are used to parametrize covalent and electrostatics forces, whereas van der Waals forces used in MD simulations are estimated using reported data from the literature.

DFT yields two dimers in staggered and shifted configurations.[2] Electronic and binding energies are summarized in Table 6 for all cases. Binding energies are calculated as the difference between twice the energy of a Li_2Pc molecule and the energy of the dimer. Both HF and DFT results indicate that the shifted dimer seems to be slightly more stable than the staggered configuration, although we also notice a large sensitivity of the results to method and basis set employed. Figure 5 shows the calculated $(Li_2Pc)_2$ structures using B3LYP/6-31G(d).[2] The shifted structure is shown in (a), and the staggered one in (b). In the shifted dimer structure, the lithium atoms above/below the Pc ring are separated by 2.23 Å, as compared with 1.99 Å in the monomer. The lithium atoms between two Pc rings are

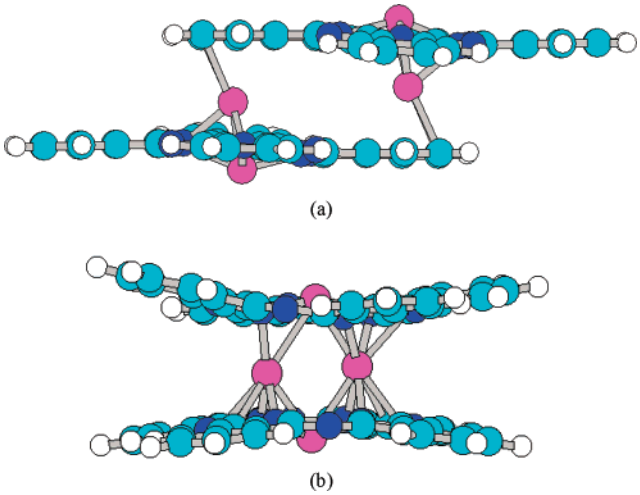

Figure 5. Optimized structures (B3LYP/6-31g(d)) of $(Li_2Pc)_2$. (a) Shifted, (b) staggered.

separated by 5.89 Å, and the distance between two Pc rings is 3.77 Å. In the staggered dimer structure, the separation between two lithium atoms that are between the two Pc rings, respectively, is 2.99 Å, whereas the separation between the Li atoms each above the Pc ring is 4.47 Å and the Pc rings are rotated approximately 30° respect to each other. The separation between the outer benzene rings in the staggered structure varies from 3.94 to 4.89 Å.

3.2. MD Simulations. *3.2.1. Structure.* The final structures (after 1200 ps total simulation length) of the four forms of Li_2Pc (Table 1) are shown in Figure 6. The corresponding Li−Li intramolecular distance (for α-, β-, ϵ-, and χ-forms) are also computed as averages and reported in Table 7. The MD results (Figure 6) indicate that molecules in the ϵ-form and the χ-form are shifted from each other in two adjacent layers, while those

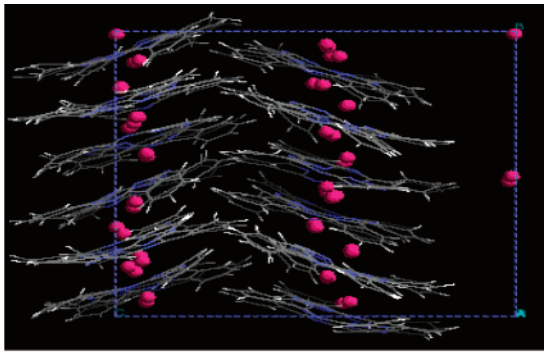

(a)

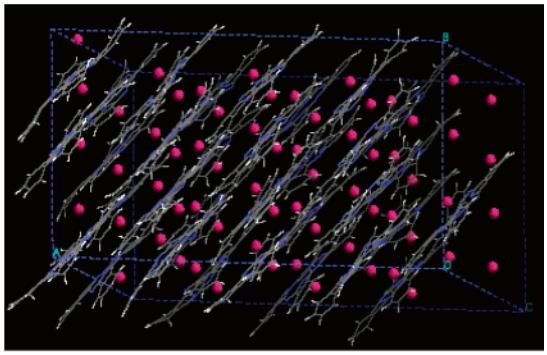

(b)

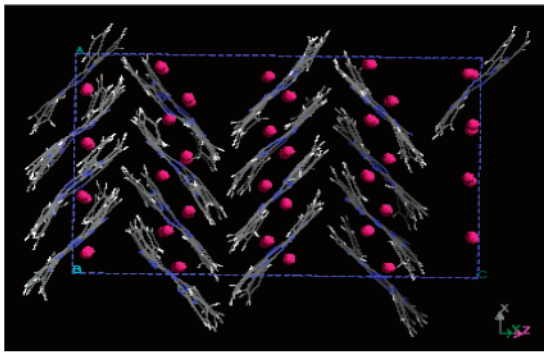

(c)

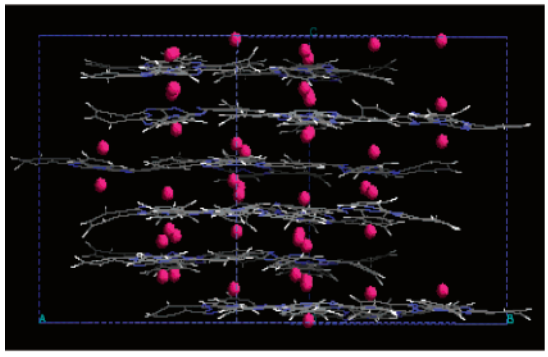

(d)

Figure 6. Structures resulting from MD after 1200 ps of production time (a) α-form, (b) β-form, (c) ϵ-form, (d) χ-form.

in the α-form and β-form are staggered. In the shifted structure, lithium atoms locate between the ring center of one molecule and one of the benzene rings of the second molecule (Figure 5a), whereas in the staggered structure, both lithium atoms locate between the ring centers of the two molecules (Figure 5b). The separations between layers (Table 7) have been computed (from the last MD configuration of each case) as averages over measured distances between all the equivalent two adjacent layers within the simulation cell. Comparison of these distances (Table 7) with those of $(Li_2Pc)_2$ calculated by B3LYP/6-31G-(d) (3.72 Å for the staggered form and 3.77 Å for the shifted form) indicates good agreement between MD and DFT regarding the staggered forms, whereas shorter distances are found by MD in the shifted configurations.

Another difference between the DFT dimer structures and the MD results arises from the intramolecular distance between two lithium atoms, which are elongated after MD (2.2−2.6 Å for ϵ- and χ-forms, and 2.4−2.9 Å for α- and β-forms, note that average values are listed in Table 7), whereas 1.99 Å, 2.23 Å, and 2.56 Å separations were found after B3LYP/6-31G(d) geometry optimization of a single molecule as well as in the shifted and staggered dimers, respectively. The longer Li−Li intramolecular distances obtained from the MD simulations in comparison with the DFT results point to the influence of collective effects of the much larger ensemble of molecules in the MD simulations, but also they may be a reflection of a weakening of the Li−N bonds which would facilitate the mobility of the lithium atoms in the self-assembled structure. On the other hand, the small energy difference found between the average total energies shown in Table 7 is an indication of possible polymorphism of Li_2Pc.

Radial distribution functions (rdf's), $g_{XY}(r)$, are indicators of local structure, defined as the ratio of the local density (at position r) of atoms Y surrounding a central atom X, with respect to the bulk density, where the local density is evaluated in spherical shells surrounding the central atom. Rdfs between Li and H, C, N, and Li, respectively, are shown in Figure 7. The first peak of the $g_{LiLi}(r)$ corresponds to intramolecular Li−Li distances (Figure 7a). For the ϵ- and χ-forms (shifted), these peaks are sharper and more intense than those of the staggered forms, and they are centered at 2.45 and 2.47 Å, respectively. For the staggered α- and β-forms, the first peak is slightly shifted to larger distances, centered at about 2.67 Å. Note, however, that the first peak of $g_{LiLi}(r)$ for the α-form presents a small shoulder approximately at 2.45 Å which may indicate that the α-form is composed of a combination of shifted and staggered structures. The second and third Li−Li peaks of $g_{LiLi}(r)$ also provide a good indication of the difference between staggered and shifted structures. The second peak of each form corresponds to two lithium atoms between two consecutive Pc rings, whereas the third peak of each form corresponds to Li57−Li57′, or Li58−Li58′ (see Figure 1). The staggered structures have their second peak located at 3.8 to 4 Å for the β- and α-forms, respectively, and a clear third peak is located at about 5 Å. In contrast, the second and third Li−Li peaks of the shifted structures are located at longer distances, about 5 and 6 Å, respectively, for the ϵ-form, whereas less long-range order is observed for the χ-form.

Figure 7b displays the Li−N rdf's, where the first peak corresponds to Li−N intramolecular interactions. The first peak at 2.3 Å in $g_{LiN}(r)$ (Figure 7b) corresponds to lithium atoms to N49, N50, N53, and N54 (Figure 1), while the second peak at 3.6 Å corresponds to lithium atoms to N51, N52, N55, N56; the position of both peaks agree for all the crystalline forms, but the second peak is less intense for the staggered structures, and a third peak is also clearly defined for all cases. The broadening of the first peak may be attributed to the contributions from two alternative structures in the staggered forms.

TABLE 7: Average Parameters of Li_2Pc Self-Assembled Structures after 700 ps of MD

Li_2Pc polymorphs	α-form	β-form	ϵ-form	χ-form
structure	staggered	staggered	shifted	shifted
density (g/cm^3)	1.40	1.40	1.51	1.40
interplanar distance (Å)[a]	3.75	3.52	3.17	3.25
Li−Li intramolecular distance (Å)[a]	2.67	2.68	2.45	2.47
energy (kJ/mol)	−1850.50	−1853.44	−1852.31	−1856.71
energy fluctuation (kJ/mol)	8.10	9.07	9.12	8.05
temperature (K)	285.60	279.26	280.68	285.05
temperature fluctuation (K)	4.33	3.66	3.70	4.30

[a] According to B3LYP/6-31G(d) optimizations, the interplanar separations in the staggered form of the dimer is 3.72 Å, and 3.77 Å for the shifted form. The Li−Li intramolecular distance in the dimer is 2.56 Å (staggered), 2.23 Å (shifted), and 1.99 Å in the monomer.

$g_{LiX}(r)$s (X = C, H) of the ϵ- and χ-forms (Figures 7c and 7d) are similar, and similarity also exists between those of the α- and β-forms. As we discussed before, in the shifted system, lithium atoms are located between the ring center of one molecule and one of the benzene rings of the second molecule. Thus, the first peak of $g_{LiX}(r)$ (X = C, H) (Figures 7c and7 d) in the ϵ- and χ-forms corresponds to lithium atoms interacting with C and H atoms, respectively, on the benzene ring mentioned above.

In the staggered system, lithium atoms are located between the centers of two phthalocyanine rings. Thus in the α- and β-forms, the first peak of $g_{LiC}(r)$ mainly corresponds to lithium atoms interacting with part of the C atoms of the inner Pc ring. Their intensity is much lower than that of the ϵ- and χ-forms, probably because there is a small degree of shifting that causes the Li ion not to be centered on the Pc ring; therefore, we detect a combination of shorter Li−C and longer Li−C intramolecular distances. Both the first and second peaks are much sharper and better defined for the shifted than for the staggered structures. Also, because of the different location of lithium atoms in the shifted and staggered systems, the first peak of $g_{LiH}(r)$ is centered at 3.2 Å in the ϵ- and χ-forms (where the Li atom is on top of the benzene ring), whereas a very low-density peak is found at 3.7 Å in the α- and β-forms.

3.2.2. X-ray Spectra. PowderCell Version 1.0,[29] a program for exploring and manipulating crystal structures and calculating X-ray powder patterns was used to calculate X-ray spectra corresponding to the simulated structures. This program uses as input primitive cell parameters and structure (atomic positions) and simulates an X-ray pattern using Bragg's law, weighting the contributions of each atom with calculated structure factors. We used as input the coordinates from the final molecular structure of the MD simulations in the primitive cells of each of the four crystalline forms, along with their respective primitive cell parameters (Table 1), to obtain simulated X-ray powder diffractograms.

Figures 8a and 8b show experimental X-ray diffraction spectra of Li_2Pc synthesized in Argonne National Laboratory (dried at 220 °C in a vacuum), and received from Aldrich (dried at 160 °C in a vacuum), respectively. Comparing the two experimental spectra, we observe that in Figure 8a several sharp peaks appear at an angle 2θ around 20°, but only a broad peak is detected in Figure 8b, where some small peaks disappear. We speculate that the experimental X-ray spectra may reflect a mixture of Li_2Pc polymorphs, some of them less crystalline than others; the presence of impurities may also add new features to the spectrum, as observed in other metal phthalocyanines.[13,30] In addition, different methods to synthesize Li_2Pc may give different mixtures of Li_2Pc polymorphs. It is also possible that structural changes may exist because of the different drying temperatures.

Figures 8c−8f show the simulated X-ray spectra for the four investigated crystalline forms. In our comparative analysis, we notice that internal molecular reorientations of the Li_2Pc molecules in a primitive cell may cause enhancement, reduction, or even disappearance of some of the peaks that would arise because of the primitive cell dimensions, and the possible influence of polymorphism in the experimental data may obscure a direct comparison of the calculated and experimental structures. However, we perform a direct comparison of each of the calculated spectrum to the experimental data (Figures 8a and 8b), assuming that the latter are single-crystalline phases.

A reasonable agreement in the peak positions is found for the ϵ-form (Figure 8e), not surprisingly since the parameters of the primitive cell of the ϵ-form were selected to reproduce the *d* spacing of the experimental diffractogram of Figure 8a; however, the agreement is less satisfactory for angles $2\theta > 20°$. The correspondence is much better for the β-form which has similar dimensions to the ϵ-cell. Moreover, comparison between the relative intensities of the simulated diffraction peaks with the experimental ones points to a better agreement of the β-form over the ϵ-form. The experimental spectra in Figures 8a and 8b, and that of the calculated β-phase (Figure 8d) show also a close similarity to the reported spectra for the β-phase of H_2Pc[30] and MgPc.[13]

On the other hand, the simulated X-ray spectrum of the α-form of Li_2Pc exhibits few and rather broad diffraction peaks, compared to other three Li_2Pc simulated polymorphs. This feature is indicative of a low crystallinity of the α-form, which was also observed for the α-forms of other metal phthalocyanines.[7,31] The fusion of the two peaks appearing in the range $5 < 2\theta < 10°$ is another characteristic of the α-phase, also detected in other metal and nonmetal phthalocyanines.[13,30] In comparison with Figures 8a and 8b, we discard the contribution of the α-phase to the experimental spectrum.

The simulated X-ray spectrum of the χ-form shows a well-defined crystalline structure. However, although some peaks appear at the same position of the experimental ones, most of them do not, and probably the χ-form is not the predominant form that contributed to the experimental data. However, the peak of highest intensity for this structure appears at a value 2θ of 18.8° in coincidence with the broad peak of Figure 8b that makes the main difference between the experimental structures Figures 8a and 8b. This aspect points to the possibility of a mixture of the most-likely β-form with the χ-form in the experimental (Figure 8b) spectrum.

In summary, the results in Figure 8 indicate that the best agreement between experimental and calculated results is found for the β-phase.

3.2.3. Ion Channel Formation and Ionic Diffusion. Looking at the self-assembly molecular organization, an alignment of lithium ions is found that can be associated with the expected

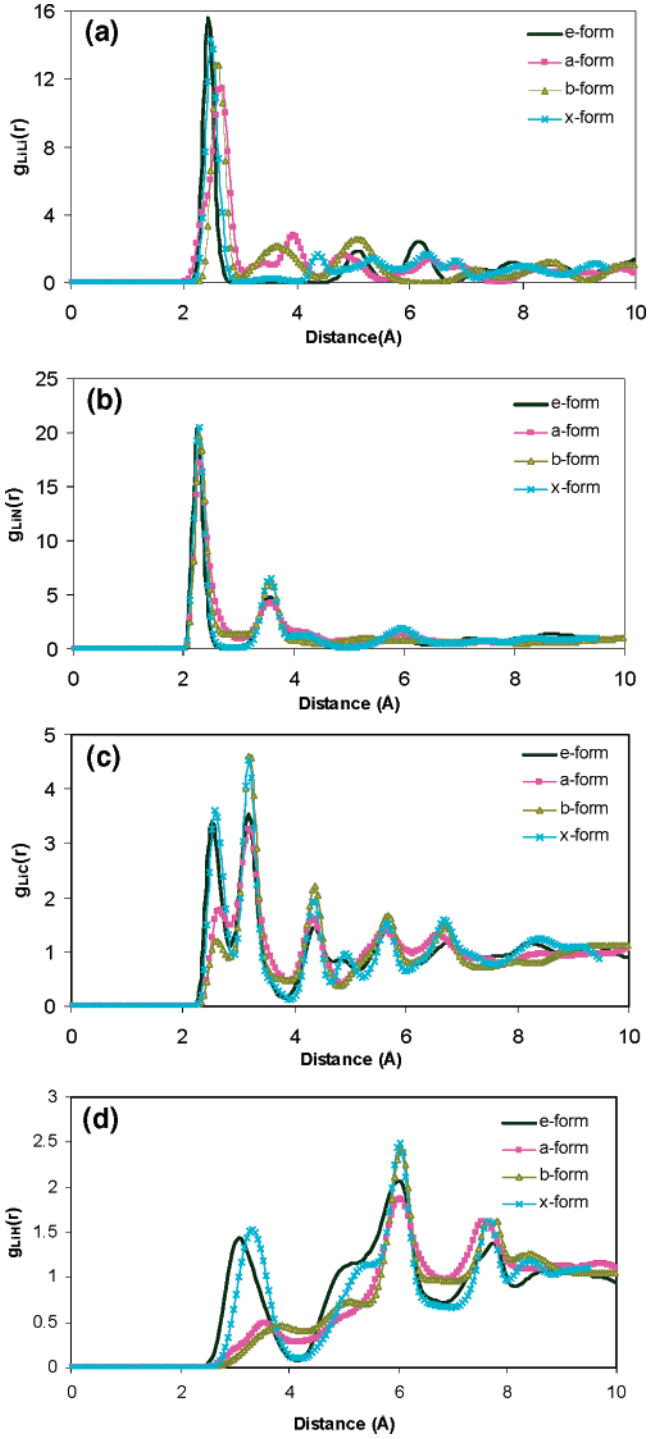

Figure 7. Partial radial distribution functions: (a) Li−Li; (b) Li−N; (c) Li−C; (d) Li−H.

lithium ion conducting channels. We can visualize these conducting channels in the α-form, β-form, and ϵ-form, when combining the top (not shown) and side (Figure 6) views of the unit cells, or rotating the unit cell of χ-form, as shown in Figure 9. These chains of ions are oriented along the same direction across layers.

To investigate lithium mobility, we calculated the velocity autocorrelation function (VAF), which is related to the macroscopic, phenomenological, self-diffusion coefficient D through the Green-Kubo formula,[32] written as the time integral of a

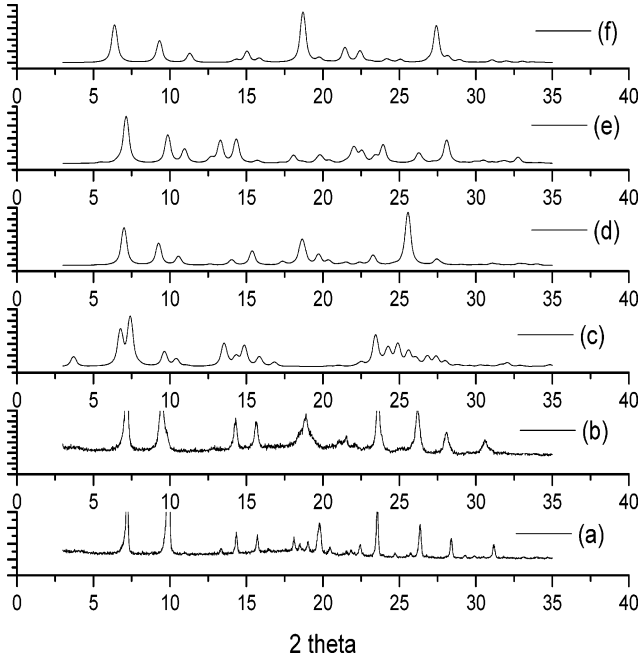

Figure 8. Comparison of simulated X-ray with experimental data. (a) Li_2Pc synthesized in Argonne National Laboratory (dried at 220 °C vacuum). (b) Li_2Pc from Aldrich (dried at 160 °C vacuum). (c) α-form, (d) β-form, (e) ϵ-form, (f) χ-form.

microscopic time-correlation function:

$$D = \int_0^\infty \langle v(t).v(t_0)\rangle_{t_0} dt \qquad (7)$$

where the function in brackets is a measure of the projection of the particle velocity at time t onto its initial value, averaged over all initial conditions t_0. Figure 10 shows the VAF for lithium ions of Li_2Pc in each of the crystalline forms in Table 1, at 300 K. The velocity autocorrelation function of lithium ions shows oscillations in the time domain, indicating the rattling motion of lithium ions in the "cage" of their nearest neighbors. The corresponding conductivity of lithium ions was calculated via the Nernst−Einstein equation,

$$\kappa = \frac{cDz^2F^2}{RT} \qquad (8)$$

where the c is the concentration of lithium ions, D is the ionic diffusion coefficient, z is the charge on lithium ions, F is the Faraday constant, R is the gas constant, and T is the absolute temperature.

The results shown in Table 8 illustrate the differences in ionic mobility imposed by the various crystal structures, with the less crystalline α-form having the smallest self-diffusion coefficient and the ϵ-form the highest. A transport mechanism for lithium ions in Li_2Pc has been suggested, whereby instead of depending on polymer segmental motion as in the PEO system,[33] the lithium ion diffusion would depend mainly on the electric field gradient in the system. Values of diffusion of lithium ions in PEO/$LiClO_4$ mixtures were reported to be 5.2×10^{-9} cm^2/s at 349 K,[34] which are below our calculated values at 300 K. Compared to the experimental ionic conductivity in Li_2Pc (Table 8), the simulated lithium ion conductivity results are about 1 order of magnitude smaller. This difference is explained considering that, in the simulation, ions move via self-diffusion determined by the field created by the self-assembly of Li_2Pc molecules, while in the experiment, diffusion across the electrolyte/electrode interface is driven by a difference of

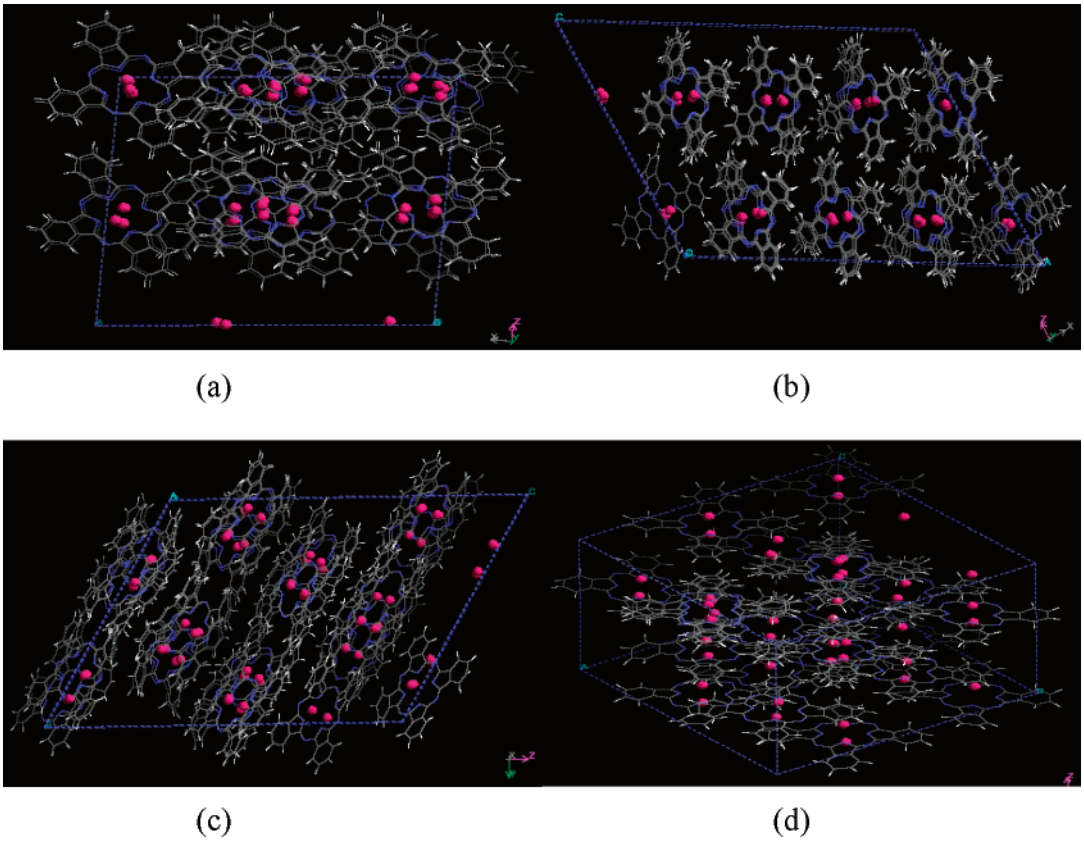

Figure 9. Structure obtained from MD showing the lithium ions diffusion channel. (a) α-form, (b) β-form, (c) ϵ-form, (d) χ-form.

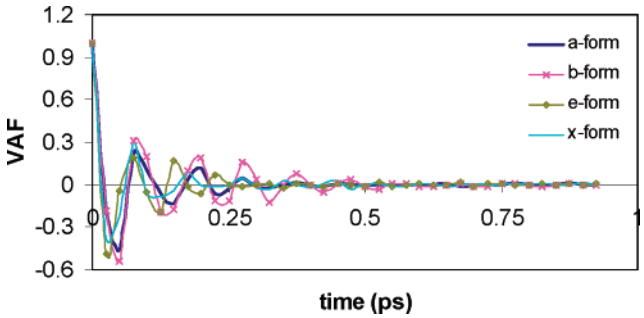

Figure 10. VAF plot for lithium ions at 300 K.

TABLE 8: Calculated Diffusion Coefficient and Conductivity of Lithium Ions in Various Li_2Pc Crystalline Forms at 300 K

Li_2Pc crystalline form	diffusion coefficient (cm^2/s)	conductivity[a] (S/cm)
a	5.94×10^{-9}	2.65×10^{-5}
b	1.35×10^{-8}	6.03×10^{-5}
ϵ	2.04×10^{-8}	9.79×10^{-5}
χ	1.88×10^{-8}	8.40×10^{-5}

[a] Experimental ionic conductivities of 5.1 to 8.9 $\times 10^{-4}$ S/cm were obtained at 300 K.[17]

chemical potential and by an electric field gradient established between the electrodes of an electrochemical cell. Work to incorporate the effect of an electric field in the simulations is in progress, and will be reported elsewhere. Further, we note that eq 7 has the implicit assumption that ions at low concentrations do not interact with each other and therefore their motion is uncorrelated. However, this is an oversimplification of this system that has a strong long-range Coulombic component. A more accurate equation would relate the conductivity to the charge flux autocorrelation function,[35] where the charge flux is calculated by the sum of charge times velocity for each ion. Alternatively, one could calculate Maxwell-Stefan diffusion coefficients, where the mass fluxes are linearly related to the gradient of chemical potential instead of being proportional to the gradient of concentration.[36]

Conclusions

Ab-initio and molecular dynamics calculations show the viability of using a large array of molecules to form a lithium ion conducting channel via molecular self-assembly. The elongation of the Li−Li intramolecular distances based on the molecular dynamics calculations illustrate collective effects provided by the self-assembled structure and their importance for facilitating fast ionic transport within the channel.

The close values of the calculated binding energies (B3LYP/6-31G(d)) for the staggered and shifted dimer structures suggest the ease of formation of various polymorphs simultaneously during material preparation, although from the comparison of the simulated and experimental X-ray data we conclude that Li_2Pc is in a predominant β-phase. On the other hand, calculated ionic conductivities are 1 order of magnitude below the experimental values, which is primarily attributed to the absence of an external driving force for ionic diffusion in the simulated self-assembled structures.

Acknowledgment. This work is supported by funds from the Air Force Research Laboratory. Supercomputer time provided by the National Energy Research Scientific Computing Center (NERSC) is gratefully acknowledged. We thank C. Johnson and G. Sandí from Argonne National Laboratory for helpful discussions.

References and Notes

(1) Scanlon, L. G.; Lucente, L. R.; Feld, W. A.; Sandi, G.; Campo, D.; Turner, A.; Johnson, C.; Marsh, R. Lithium-ion conducting channel. In *Proceedings of the International Workshop on Electrochemical Systems*; Landgrebe, A. R., Klingler, R. J., Eds.; 2000; Vol. 36, p 326.

(2) Scanlon, L. G.; Lucente, L. R.; Feld, W. A.; Sandi, G.; Balbuena, P. B.; Alonso, P. R.; Turner, A. Composite cathode with Li_2Pc. *J. Electrochem. Soc.*, in press.

(3) Fischer, M. S.; Templeton, D. H.; Zalkin, A.; Calvin, M. Structure and Chemistry of the Porphyrins. The Crystal and Molecular Structure of the Monohydrated Dipyridinated Magnesium Phthalocyanin Complex. *J. Am. Chem. Soc.* **1971**, *93*, 2622.

(4) Diel, B. N.; Inabe, T.; Lyding, J. W.; Schoch, K. F. J.; Kannewurf, C. R.; Marks, T. J. Cofacial Assembly of Partially Oxidized Metallomacrocycles as an Approach to Controlling Lattice Architecture in Low-Dimensional Molecular Solids. Chemical, Structural, Oxidation State, Transport, Magnetic and Optical Properties of Halogen-Doped $[M(phthalocyaninato)O]_n$ Macromolecules, Where M = Si, Ge, and Sn. *J. Am. Chem. Soc.* **1983**, *105*, 1551.

(5) Dirk, C. W.; Inabe, T.; Schoch, K. F. J.; Marks, T. J. Cofacial Assembly of Partially Oxidized Metallomacrocycles as an Approach to Controlling Lattice Architecture in Low-Dimensional Molecular Solids. Chemical and Architectural Properties of the "Face-to-Face" Polymers $[M(phthalocyaninato)O]_n$ Where M = Si, Ge, and Sn. *J. Am. Chem. Soc.* **1983**, *105*, 1539.

(6) Sugimoto, H.; Mori, M.; Masuda, H.; Taga, T. Synthesis and molecular structure of a lithium complex of phthalocyanine radical. *J. Chem. Soc., Chem. Commun.* **1986**, 962.

(7) Brinkmann, M.; Chaumont, C.; Wachtel, H.; Andre, J. J. Polymorphism in powders and thin films of lithium phthalocyanine. An X-ray, optical, and electron spin resonance study. *Thin Solid Films* **1996**, *283*, 97.

(8) Andre, J. J.; Brinkmann, M. Molecular semiconductors for magnetometry and oximetry: lithium phthalocyanine radical. *Synth. Met.* **1997**, *90*, 211.

(9) Brinkmann, M.; Turek, P.; Andre, J. J. EPR study of the χ-, α- and β-structures of lithium phthalocyanine. *J. Mater. Chem.* **1998**, *8*, 675.

(10) Ilangovan, G.; Zweier, J. L.; Kuppusamy, P. Electrochemical Preparation and EPR Studies of Lithium Phthalocyanine: Evaluation of the Nucleation and Growth Mechanism and Evidence for Potential-Dependent Phase Formation. *J. Phys. Chem. B* **2000**, *104*, 4047.

(11) Kimura, T.; Sumimoto, M.; Sakaki, S.; Fujimoto, H.; Hashimoto, Y.; Matsuzaki, S. Electronic structure of lithium phthalocyanine studied by ultraviolet photoemission spectroscopy. *Chem. Phys.* **2000**, *253*, 125.

(12) Yanagi, H.; Manivannan, A. Epitaxial growth of molecular magnetic thin films of lithium phthalocyanine. *Thin Solid Films* **2001**, *393*, 28.

(13) Janczak, J.; Kubiak, R. X-ray single-crystal investigations of magnesium phthalocyanine. The 4+1 coordination of the Mg ion and its consequence. *Polyhedron* **2001**, *20*, 2901.

(14) Wachtel, H.; Wittmann, J. C.; Lotz, B.; Petit, M. A.; Andre, J. J. Anisotropic spin transport in oriented lithium phthalocyanine thin films, *Thin Solid Films* **1994**, *250*, 219.

(15) Homborg, H.; Teske, C. L. Lithium phthalocyanines: preparation and characterization of the monoclinic and tetragonal modifications of LiPc(1-) and the halogen adducts LiPc(1-)X (X = Cl, Br, I). *Z. Anorg. Allg. Chem.* **1985**, *527*, 45.

(16) Johnson, C. Private communication.

(17) Scanlon, L. G. Private communication.

(18) Frisch, M. J.; Trucks, G. W.; Schlegel, H. B.; Scuseria, G. E.; Robb, M. A.; Cheeseman, J. R.; Zakrzewski, V. G.; Montgomery, J. A.; Stratmann, R. E.; Burant, J. C.; Dapprich, S.; Millam, J. M.; Daniels, A. D.; Kudin, K. N.; Strain, O. F. M. C.; Tomasi, J.; Barone, B.; Cossi, M.; Cammi, R.; Mennucci, B.; Pomelli, C.; Adamo, C.; Clifford, S.; Ochterski, J.; Petersson, G. A.; Ayala, P. Y.; Cui, Q.; Morokuma, K.; Malick, D. K.; Rabuck, A. D.; Raghavachari, K.; Foresman, J. B.; Ciolovski, J.; Ortiz, J. V.; Stefanov, V. V.; Liu, G.; Liashensko, A.; Piskorz, P.; Komaroni, I.; Gomperts, R.; Martin, R. L.; Fox, D. J.; Keith, T.; Al-Laham, M. A.; Peng, C. Y.; Nanayakkara, A.; Gonzalez, C.; Challacombe, M.; Gill, P. M. W.; Johnson, B.; Chen, W.; Wong, M. W.; Andres, J. L.; Head-Gordon, M.; Replogle, E. S.; Pople, J. A. *GAUSSIAN 98*, Revision A.11; Gaussian Inc.: Pittsburgh, PA, 1998.

(19) Shirley, R. *The CRYSFIRE System for Automatic Powder Indexing: User's Manual*; The Lattice Press: Guildford, Surrey GU2 7NL, England, 2000.

(20) Rappe, A. K.; Casewit, C. J.; Colwell, K. S.; Goddard, W. A.; Skiff, W. M. UFF, a full periodic table force field for molecular mechanics and molecular dynamics simulations. *J. Am. Chem. Soc.* **1992**, *114*, 10024.

(21) *Molecular Simulations, I*; CERIUS 2: San Diego, CA, 1997.

(22) Smith, W.; Forester, T. R. DL_POLY; Daresbury Laboratory: Daresbury, 1996.

(23) Mayo, S. L.; Olafson, B. D.; Goddard, W. A. Dreiding: A generic force field for molecular simulations. *J. Phys. Chem.* **1990**, *94*, 8897.

(24) Heizinger, K. *Pure Appl. Chem.* **1985**, *57*, 1031.

(25) Allen, M. P.; Tildesley, D. J. *Computer Simulation of Liquids*; Oxford University Press: Oxford, 1990.

(26) Mulliken, R. S. Electronic population analysis on LCAO-MO molecular wave functions. I. *J. Chem. Phys.* **1955**, *23*, 1833.

(27) Mulliken, R. S. Electronic population analysis on LCAO-MO molecular wave functions. II. Overlap populations, bond orders, and covalent bond energies. *J. Chem. Phys.* **1955**, *23*, 1841.

(28) Mulliken, R. S. Electronic population analysis on LCAO-MO molecular wave functions. III Effects of hybridization on overlap and gross AO populations. *J. Chem. Phys.* **1955**, *23*, 2338.

(29) Kraus, W.; Nolze, G. PowderCell for Windows; Federal Institute for Materials Research and Testing: Berlin, Germany, 1997.

(30) Kubiak, R.; Janczak, J.; Ejsmont, K. On polymorphic and non-polymorphic conversions of phthalocyanines. *Chem. Phys. Lett.* **1995**, *245*, 249.

(31) Assour, J. M.; Harrison, S. E. Electron spin resonance of concentrated copper phthalocyanine crystals. *Phys. Rev.* **1964**, *136*, 1368.

(32) Hansen, J.-P.; McDonald, I. R. *Theory of simple liquids*, 2nd. ed.; Academic Press: San Diego, CA, 1990.

(33) Kuppa, V.; Manias, E. Computer Simulation of PEO/Layered-Silicate Nanocomposites: 2. Lithium Dynamics in PEO/Li+ Montmorillonite Intercalates. *Chem. Mater.* **2002**, *14*, 2171.

(34) Gorecki, W.; Andreani, R.; Berthier, C.; Armand, M.; Mali, M.; Roos, J.; Brinkmann, D. NMR, DSC, and conductivity study of a poly(ethylene oxide) complex electrolyte: $PEO(LiClO_4)_x$. *Solid State Ionics* **1986**, *18−19*, 295.

(35) Muller-Plathe, F.; vanGunsteren, W. F. Computer simulation of a polymer electrolyte: Lithium iodide in amorphous poly(ethylene oxide). *J. Chem. Phys.* **1995**, *103*, 4745.

(36) Thompson, A. P.; Heffelfinger, G. S. Direct molecular simulation of gradient-driven diffusion of large molecules using constant pressure. *J. Chem. Phys.* **1999**, *110*, 10693.